Preprints of the 21st IFAC World Congress (Virtual)
Berlin, Germany, July 12-17, 2020

A Fractional Order SMC approach to Improve the Reliability of Wind Energy Systems During Grid Faults

Md Nafiz Musarrat*. Afef Fekih*

Department of Electrical and Computer Engineering, University of Louisiana at Lafayette, Lafayette, Louisiana, USA, (e-mails: md-nafiz.musarrat1@louisiana.edu, afef.fekih@louisiana.edu)

Abstract: This paper proposes a fractional order sliding mode approach for the converters of a DFIG-based wind energy system. It aims at mitigating grid faults and improving power reliability in the presence of uncertainties and sudden load variations. Its reliance on fractional calculus results in smoother control actions and reduced chattering compared to standard SMC. It also implements a super-capacitor as energy storage for its faster response compared to a conventional battery. The proposed approach was validated using a DFIG-based wind energy system installed in a small-scale standalone power supply network. Its performance was further compared to that of a standard PI approach. The obtained results showed significant improvement in the performance of the wind energy system during grid faults.

Keywords: DFIG, grid fault, reliability, crowbar, fractional order sliding mode control, super-capacitor, supplemental energy storage, bidirectional converter.

NOMENCLATURE

WECS	Wind Energy Conversion System.
WT	Wind Turbine.
DFIG	Doubly Fed Induction Generator.
RSC, (GSC)	Rotor Side Converter (Grid Side Converter)
FRT	Fault Ride Through
SMC	Sliding Mode Control.
PI	Proportion Integral.
FOSMC	Fractional Order Sliding Mode Control.
PWM	Pulse Width Modulation.
PCC	Point of Common Coupling.
P_s (Q_s)	Active (reactive) stator power.
P_{dfig} (Q_{dfig})	Total active (reactive) power from DFIG.
P_{GSC} (Q_{GSC})	Active (reactive) power from GSC.
V_{gd} (V_{gq})	Direct (quadrature) components of the GSC voltage.
i_{gd} (i_{gq})	Direct (quadrature) components of the GSC current.
i_{rd} (i_{rq})	Direct (quadrature) components of the rotor current.
V_{rd} (V_{rd})	Direct (quadrature) components of the rotor voltage.
V_{sd} (V_{sd})	Direct (quadrature) components of the stator voltage.
M	Mutual inductance.
ψ_{sd} (ψ_{sq})	Direct (quadrature) components of the stator flux.
R_s (R_r)	Stator (rotor) resistance.
L_s (L_r)	Stator (rotor) inductance.
L_r(R_r)	Stator (rotor) resistance.
ω_s (ω_r)	Stator (rotor) electric angular pulsation.

1. INTRODUCTION

Wind energy is one of the most promising sustainable energy sources which worldwide capacity has reached 597 GW by the end of 2018 (Chen (2019)). Due to various attributes, such as speed variability, lower rated inverter, and decoupled control of active and reactive power control capability, DFIGs are vastly popular as wind energy systems. As depicted in Fig. 2, these latter achieve their variable speed operation via two back to back voltage source converters; RSC and GSC. The direct connection of the converters to the grid, however, makes them vulnerable to grid faults. These are short duration reductions in rms voltage triggered by either short circuits, overloading or load fluctuations. When faults occur, they result in a sudden short circuit current in the stator coils. Since this latter is magnetically coupled with the rotor coils, the fault will result in a sudden rise in rotor currents by as much as two to three times the nominal range (Erlich et al. (2007)). These high currents are not acceptable since they might damage the back to back converter system. Further, high rotor currents lead to a considerably fast rise in dc-link voltage by as much as 2-3 times the nominal voltage which is well beyond the system rating. Furthermore, when faults occur, the drive train experiences a highly oscillating torque due to sudden change in dc-link voltage and the reliability of the turbine shaft reduces. Thus, devising fast and efficient measures to protect the converters during faults is essential in maintaining the reliable operation of wind turbines and preventing such faults from causing a widespread loss of generation, especially in stand-alone power supply systems, where grid disturbances are quite frequent.

Active power and voltage support are very important, especially during grid faults. Crowbar is the most popular protection technique against grid faults. It operates by isolating the rotor side converter from the rotor coil current. However, with crowbar activation, the DFIG merely becomes a normal induction generator and the RSC loses its controllability. Additionally, crowbar activation results in a significant amount of reactive power consumption (Zhang et al. (2011)), thus further worsening the voltage sag condition at the point of common coupling (PCC). It is to be mentioned that the crowbar is triggered by the sudden rise in the dc-link voltage beyond the threshold limit. Since the high rotor current during fault causes damage to the IGBT switches in the rotor side converter, protection schemes are systematically installed to every converter module as protection measure. During current surges, the IGBT switches are bypassed by the protection system, however the high rotor current and energy will still flow through the freewheeling diodes. This will cause a very fast increase in

the dc-link voltage. If the dc-link voltage can be regulated near the rated value, the crowbar triggering can be avoided. Even after the fault is cleared, the crowbar may be triggered as sudden voltage recovery results in a rise in the dc-link voltage which could trigger the crowbar system thus leading to more reactive power consumption. Additionally, the sudden activation of the crowbar causes a very high transient in the electromagnetic torque, thus resulting in significant stress on the drive train. Therefore, it is desirable to improve the system's fault ride through capability with minimum crowbar triggering.

Various alternative strategies to crowbar have been investigated in the literature. A strategy integrating a dc chopper in the dc-link to improve the FRT capability of a DFIG-based wind turbine was proposed in reference (Jalilian et al. (2017)). The authors in reference (Yang et al. (2010)) proposed implemented series dynamic breaking resistors in the rotor circuit to offset the high rotor current during fault. In reference (Naderi et al. (2017)), fault current limiter has been utilized to limit the dc-link voltage surge. Another group of strategies incorporating the energy storage integrated with the dc-link working as a spinning reserve have been proposed in references (Aktarujjaman et al. (2006); Abbey et al. (2006)). Although, incorporating energy storage support can have a faster recovery time than the crowbar protection and is able to maintain the dc-link voltage in a close range so that the machine dynamics are only minimally hampered during network events (Mellincovsky et al. (2018)), it is often not able to provide enough support during fault to bypass the crowbar activation. Most of the existing fault ride through control approaches are (PI)-based. Though easy to implement, these control schemes are not fast enough to track random and sudden changes in the system dynamics. Additionally, they are sensitive to external disturbances which often compromise their reliability. To alleviate those problems, several nonlinear control schemes have been proposed for WECS control (Raju et al. (2016), Zhang et al. (2018), Yang et al. (2018)). Most recently, attributes such as invariance to external disturbances, robustness to uncertainties, ease of implementation with power electronics have made sliding mode control an attractive candidate for dc-link voltage maintenance and direct power control (Hu et al. (2010)). The chattering phenomena, however, caused by the discontinuous nature of the control input greatly compromises the reliability of the WECS and leads to high frequency vibrations. To solve this problem, linear hyper-lanes have been replaced by non-linear switching manifolds in terminal sliding mode control (TSMC). However, while TSMC provides asymptotic stability, it cannot ensure that the error dynamics will be converged to zero in finite time (Morshed et al. (2015)). FOSMC has recently emerged as a promising approach (Xiong et al. (2020)). The utilization of fractional calculus provides an extra degree of freedom for the sliding manifold and improve the robustness and accuracy of the controller. Additionally, fractional calculus properties contribute to a reduction in chattering compared to the classical SMC (NasimUllah et al. (2017))

This paper proposes an FOSMC-based control strategy for the converters of a DFIG-based wind turbine. Its main contributions are as follows:

- An FOSMC-based control design to mitigate grid faults and improve the power reliability of wind energy systems.
- A design that regulates the dc-link voltage to near its rated value during grid faults thus bypassing the crowbar system.

The remainder of the paper is structures as follows. Section 2 describes the state space modelling of the system. Section 3 illustrates the FOSMC design. The performance of the proposed approach is assessed and compared to that of a standard PI approach in section 4. Some conclusions are drawn in section 5.

2. SYSTEM MODELLING

2.1. Modelling of the Rotor Side Converter

Under the assumption of balanced and symmetrical system, the state space model of the DFIG in the synchronously rotating reference frame (*d-q*) (Pena et al. (1996)) is given by:

$$\dot{X}_R = f(x,t) + g(x,t)u \tag{1}$$

Where:

$$f(x,t) = \begin{bmatrix} \left\{ -\frac{R_r}{(\sigma L_r)^2}\left(\sigma L_r i_{r,d} + \frac{MV_{s,q}}{\omega_s L_s}\right) \right. \\ \left. + \frac{R_r M \psi_{s,d}}{L_s(\sigma L_r)^2} + \frac{\omega_r}{\sigma L_r}\left(\sigma L_r i_{r,q} + \frac{MV_{s,d}}{\omega_s L_s}\right) \right\} \\ \left\{ -\frac{R_r}{(\sigma L_r)^2}\left(\sigma L_r i_{r,q} + \frac{MV_{s,d}}{\omega_s L_s}\right) + \right. \\ \left. \frac{R_r M \psi_{s,q}}{L_s(\sigma L_r)^2} + \frac{\omega_r}{\sigma L_r}\left(\sigma L_r i_{r,d} + \frac{MV_{s,q}}{\omega_s L_s}\right) \right\} \end{bmatrix} \tag{2}$$

$$g(x,t) = \begin{bmatrix} \frac{1}{\sigma L_r} & 0 \\ 0 & \frac{1}{\sigma L_r} \end{bmatrix}$$

The state space matrix, $X_R = \begin{bmatrix} i_{r,d} & i_{r,q} \end{bmatrix}^T$.

The input matrix, $\begin{bmatrix} u_{r,d} & u_{r,q} \end{bmatrix}^T = \begin{bmatrix} V_{r,d} & V_{r,q} \end{bmatrix}^T$

$$\sigma = 1 - \frac{M^2}{L_s L_r} \tag{3}$$

Orienting the flux vector along the *d* axis yields:

$$\psi_{s,d} = \psi_s; \psi_{s,q} = 0;\ V_{s,d} = 0;\ V_{s,q} = V_s = \omega_s \psi_s \tag{4}$$

Hence, the state vector can be expressed as below.

$$\dot{X}_R = f_2(x,t) + g(x,t)u\ ,$$

where:

$$f_2(x,t) = \begin{bmatrix} \underbrace{-\frac{R_r}{(\sigma L_r)^2}\left(\sigma L_r i_{r,d} + \frac{MV_s}{\omega_s L_s}\right) + \frac{R_r M \psi_s}{L_s(\sigma L_r)^2} + \omega_r i_{r,q}}_{F_{r,d}} \\ \underbrace{\frac{R_r}{\sigma L_r} i_{rq} - \frac{\omega_r}{\sigma L_r}\left(\sigma L_r i_{r,d} + \frac{M}{\omega_s L_s} V_{s,q}\right)}_{F_{r,q}} \end{bmatrix} \tag{5}$$

2.2. Modelling of the Grid Side Converter

The main purpose of the grid side converter is to regulate the dc-link voltage and the fluctuation of the total active and reactive power being injected into the bus. The GSC can be expressed in a synchronous *d-q* frame as below.

$$\begin{cases} \dfrac{di_{g,d}}{dt} = \dfrac{1}{L_g}\left(V_{s,d} - R_g i_{g,d} + \omega_s L_g i_{g,q}\right) - \dfrac{1}{L_g} V_{g,d} \\ \dfrac{di_{g,q}}{dt} = \dfrac{1}{L_g}\left(V_{s,q} - R_g i_{g,q} + \omega_s L_g i_{g,qd}\right) - \dfrac{1}{L_g} V_{g,q} \end{cases} \tag{6}$$

The state space matrix, $X_G = \begin{bmatrix} i_{g,d} & i_{g,q} \end{bmatrix}^T$.

The input matrix, $\begin{bmatrix} u_{g,d} & u_{g,q} \end{bmatrix}^T = \begin{bmatrix} V_{g,d} & V_{g,q} \end{bmatrix}^T$

For the above DFIG-based wind energy conversion system, a FOSMC based robust control approach in proposed and implemented to the bi-directional converter with the aim of improving system reliability during grid faults to maintain the currents and induced torque within the allowable limit.

2.3 Modelling of the bi-directional buck-boost converter

The basic operation of the bidirectional converter can be looked as a piecewise switched dynamical system with two switching modes. The two switches are Q_1 and Q_2 as shown in Fig. 1. The input voltage v_{in} is the input voltage of the energy Storage. v_0 is the voltage at the bidirectional converter terminal which needs to be regulated. L is the inductance of the converter and C_1, C_2 are the source side and load side capacitor, respectively. It is assumed that the bidirectional converter is an ideal circuit. u is the control signal. When u=1, Q_1 is on and Q_2 is off. When control signal u=0, Q_1 is off and Q_2 is on. Two variables are considered here; the inductor current i_L and the terminal voltage v_0.

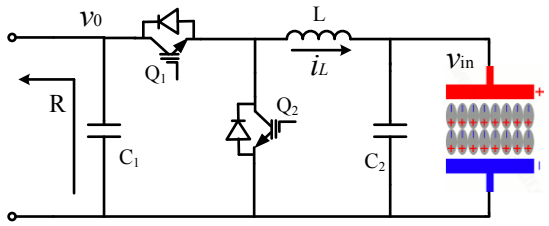

Fig. 1. A simplified topology of the bi-directional dc/dc converter with super-capacitor as an input voltage source.

Combining the state space matrices in both modes (u=1 and u=0) yields:

$$\begin{bmatrix} \dfrac{di_L}{dt} \\ \dfrac{dv_o}{dt} \end{bmatrix} = \begin{bmatrix} 0 & \dfrac{u}{L} \\ -\dfrac{u}{C} & -\dfrac{1}{RC} \end{bmatrix} \begin{bmatrix} i_L(t) \\ v_o(t) \end{bmatrix} + \begin{bmatrix} -\dfrac{1}{L} \\ 0 \end{bmatrix} v_{in}(t) \tag{7}$$

Considering the output voltage error $x_1 = v_o - v_o^{ref}$ and its derivative, x_2 as the state variables yields the following state space model:

$$\begin{bmatrix} \dot{x}_1 \\ \dot{x}_2 \end{bmatrix} = \begin{bmatrix} 0 & 1 \\ \dfrac{u}{LC} & -\dfrac{1}{RC} \end{bmatrix} \begin{bmatrix} x_1 \\ x_2 \end{bmatrix} + \begin{bmatrix} 0 \\ uv_{in} + uv_o^{ref} \end{bmatrix} \frac{1}{LC} \tag{8}$$

Where, v_o^{ref} is the reference output voltage.

3. FOSMC-BASED CONTROL PARADIGM

3.1 FOSMC Design

The conventional terminal sliding mode control can be described as

$$s = \alpha x_1^{\beta} + x_2 \tag{9}$$

Where α and β are positive integers. The dynamics of the sliding manifold is given by

$$\dot{s} = \alpha\beta n_1^{\beta-1}\dot{x}_1 + \dot{x}_2 \tag{10}$$

$$\dot{s} = \alpha\beta x_1^{\beta-1} x_2 + \frac{u}{LC}(x_1 + v_{in} + v_{ref}) - \frac{x_2}{RC} = 0 \tag{11}$$

The equivalent control can be expressed as

$$u_{eq} = \frac{(\dfrac{x_2}{RC} - \alpha\beta_{n_1}^{\beta-1} x_2)}{x_1 + v_{in} + v_o^{ref}} LC \tag{12}$$

The fractional order sliding manifold can be defined as

$$s = \alpha x_1^{\beta} + {}_{t0}D_t^{\eta-1} x_2 \tag{13}$$

D_t is the fractional calculus derivative operator. Where, in the order of the fractional derivative, $\eta \in \{0,1\}$, α is a design constant and $\beta = q/p$. Both α and β are positive odd integers satisfying $0 < q/p < 1$.

For the bidirectional converter, the control signal in fractional order sliding mode control is defined by:

$$u = \frac{(\dfrac{x_2}{RC} - D^{1-\mu}\alpha\beta_{x_1}^{\beta-1} x_2)}{x_1 + v_{in} + v_o^{ref}} LC - kSign(s) - ks \tag{14}$$

Where, $0<\beta<1$, $k>0$, $0<\eta<1$ state that x_1 and x_2 will converge to zero in finite time.

Proof: Define the following Lyapunov function:

$$v = \frac{1}{L} s^2 \tag{15}$$

Deriving (20), yields:

$$\dot{v} = s\dot{s} = s(\alpha\beta x_1^{\beta-1}\dot{x}_1 + D^{\mu-1}\dot{x}_2) \tag{16}$$

$$\dot{v} = s\alpha\beta n_1^{\beta-1} x_2 + sD^{\mu-1}\left[\frac{u}{LC}\left[x_1 + v_o^{ref} + v_{in}\right] - \frac{x_2}{RC}\right] \tag{17}$$

Substituting (21) into (19) yields:

$$\dot{v} = s(-kSign(s) - ks) = -k(|s| + s^2) \tag{18}$$

(18) shows that the control system converges in finite time. When the system reaches the sliding manifold, its dynamics can be expressed by

$${}_0D_{t_s}^{\mu-1}\dot{x}_1 = -\alpha_0 x_1^{\beta} \tag{19}$$

Taking into account the fractional integral and derivative operators, the following equation can be obtained.

$${}_0D_{t_s}^{1-\mu}({}_0D_{t_s}^{\mu-1}\dot{x}_1) = -\alpha\, {}_0D_{t_s}^{1-\mu} x_1^{\beta} \tag{20}$$

From the definition of fractional calculus (Yang, N et al.),

$$\dot{x}_1(t) - \left[{}_0D_t^{\mu-2}\dot{x}_1(t)\right]_{t=0} \frac{(t-t_r)^{\mu-2}}{\Gamma(\mu-1)} = -\alpha\, {}_0D_{t_s}^{1-\mu} x_1^{\beta}(t) \tag{21}$$

Where $\left[{}_0D_t^{\mu-2}\dot{x}_1(t)\right]_{t=0} \dfrac{(t-t_r)^{\mu-2}}{\Gamma(\mu-1)} = 0$.

Thus, it can be concluded that:

$$\dot{x}_1(t) = -\alpha\, {}_0D_{t_s}^{1-\mu} x_1^{\beta}(t) \tag{22}$$

From Riemann-Liouville definition of the α^{th} order fractional order derivative operator is expressed by (Podlubny et al. (1999))

$$D^{1-\mu}x_1^{\beta}(t)=\frac{\Gamma(\beta+1)}{\Gamma(\beta+\mu)}x_1^{\beta+\mu-1}(t) \tag{23}$$

Substituting (23) into (22) yields:

$$\dot{x}_1(t)=-\frac{\alpha\Gamma(\beta+1)}{\Gamma(\beta+\mu)}x_1^{\beta+\mu-1}(t) \tag{24}$$

Equation (29) can be rewritten as:

$$dx_1(t)=-\frac{\alpha\Gamma(\beta+1)}{\Gamma(\beta+\mu)}x_1^{\beta+\mu-1}(t)dt \tag{25}$$

Integrating both sides of (29) yields,

$$\int_0^{t_s}x_1^{1-\beta-\mu}(t)dx_1(t)=\frac{\alpha\Gamma(\beta+1)}{\Gamma(\beta+\mu)}\int_0^{t_s}dt \tag{26}$$

The finite time t_s is obtained by

$$t_s=\frac{\Gamma(\beta+\mu)x(0)^{2-\mu-\beta}}{\alpha\Gamma(\beta+1)(2-\mu-\beta)} \tag{27}$$

Hence, system trajectories are guaranteed to reach the equilibrium in finite time.

3.2 DC-link voltage regulation with super-capacitor

As mentioned earlier, despite the internal protection scheme of the rotor side converter, the dc-link and the GSC will be highly overloaded without the activation of the crowbar. Since the internal protection system of RSC already bypasses the high rotor current from the IGBT switches, controlling the dc-link voltage to remain near the nominal value during faults will maintain the system reliability as in pre-fault conditions.

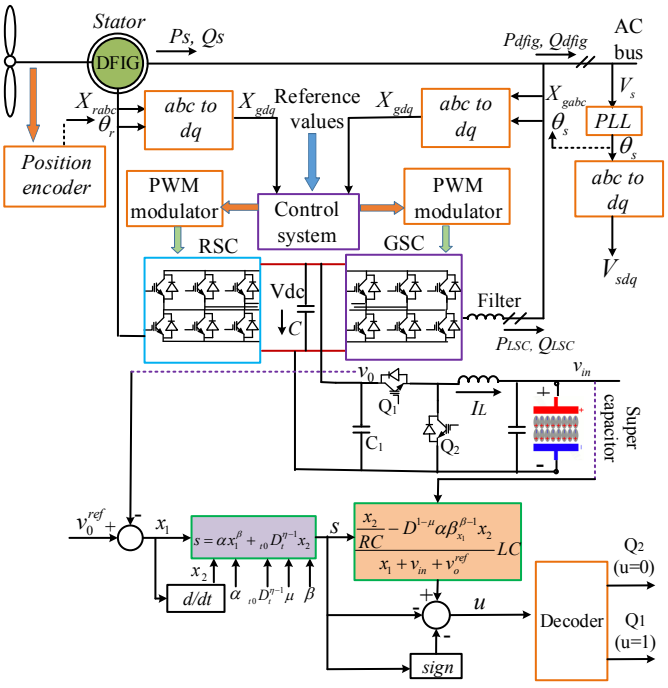

Fig. 2. Proposed control topology for dc-link voltage regulation with super-capacitor.

The schematic of the proposed strategy and topology for the bidirectional converter is depicted in Fig. 2. Note that although the aim of the proposed control strategy is to avoid the triggering of the crowbar, this latter will be available as a secondary protective measure. It will only be activated in emergency cases when the proposed controller fails to mitigate the dc-link voltage surge. Additionally, the control system needs to be effective so that the dc-link voltage is not only maintained at nominal level during the fault but also the response time needs to be fast enough so that the transient dc-link voltage during the fault's start and clearance is maintained at its pre-specified limit to avoid triggering the crowbar. To ensure fast response, a super-capacitor is used as the energy storage. Also, FOSMC control is implemented for the bidirectional converter switching to control the energy supplement from the super-capacitor since FOSMC shows better transient responses. When a fault occurs at pcc, the grid short circuit current will drastically increase the dc-link voltage. The support from the super-capacitor will help minimize the fluctuations of the dc-link voltage. Since the super-capacitor is a voltage source, the topology of the bidirectional converter should be suitable for controlling the voltage.

The dc-link voltage at the power conditioning circuit terminal is the voltage that would be regulated by the dc/dc converter. The terminal voltage will be regulated to the fixed rated dc-link voltage. When the control signal u=1, the switch Q_1 will be on and Q_2 will be off. The converter will then work as a buck converter. In this case, the super-capacitor will be charging. On the other hand, if the control signal u=0, then Q_2 will be on and Q_1 will be off. The converter will work as a boost converter. The switching of Q_1 and Q_2 is mutually exclusive. The switching of the converter is determined by the FOSMC controller. v_0 is the bidirectional converter output voltage at the dc-link which needs to be regulated to reference output voltage v_0^{ref} which is equal to nominal dc-link voltage. This strategy can be used for smoothing the output power for DFIG as well during wind fluctuations. However, the focus of this paper is only given for grid fault condition. During faulty conditions, the super-capacitor absorbs a significant amount of current from the dc-link to maintain the dc-link voltage within the specified limit. The control block diagram for the bidirectional buck-boost converter for the super capacitor operation is illustrated in Fig. 2. Initial fractional order calculus parameters and state space variables are fed into the system to form a switching manifold. From this switching manifold, appropriate control signal is established to ensure the switching of the dc/dc bidirectional converter so as to follow the reference signal.

5. COMPUTER EXPERIMENTS

The proposed control technique is implemented to the small-scale power supply test network depicted in Fig. 3. This network consists of a conventional asynchronous generator and a DFIG-based wind turbine which parameters are illustrated in the Appendix.

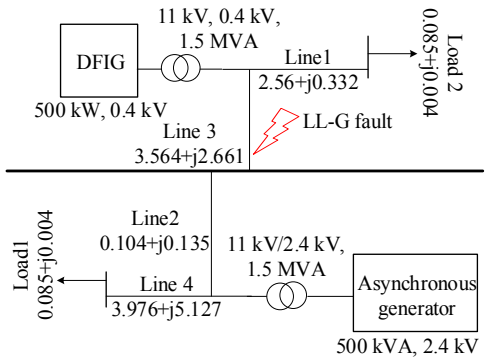

Fig. 3. Small scale power supply test network used for the validation of the proposed strategy (Tan et al.).

For comparison purposes, the following conventional PI control-based switching for the bidirectional converter is considered: $D = (v_0^{ref} - v_0)(K_p + \frac{K_i}{s})$ (28)

Where D is the duty ratio of the switching pulse and K_p, K_i are respectively the proportional and integral gains. The controller gains for the PI controller are chosen as follows: K_p= 62 and K_i= 0.3 (Naderi *et al.*, 2017). The parameters for the FOSMC controller are selected as follows: α=100, β=0.6, and μ= 0.7. A fixed switching frequency is considered with PWM modulation. The carrier frequency of 15 kHz is considered.

To assess the performance of the proposed approach under faulty conditions, we consider a double line to ground (LL-G) fault near the bus to which the DFIG is connected (Fig. 4(a)).

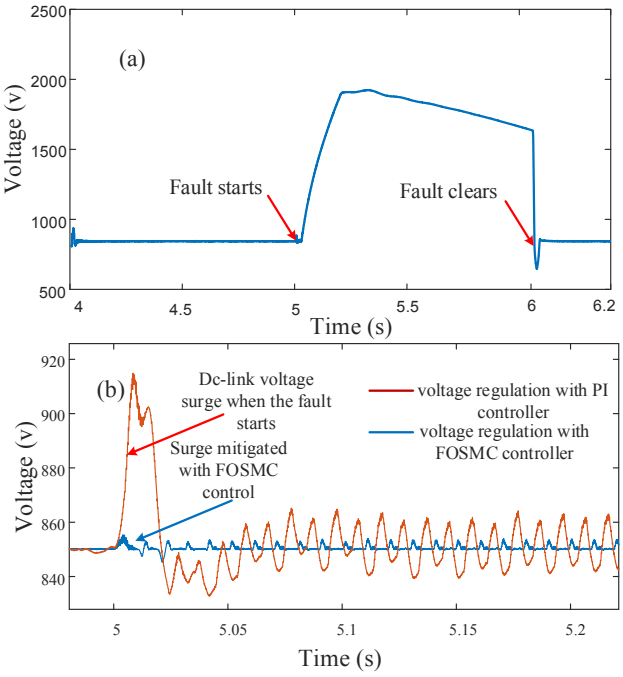

Fig. 4. Dc-link voltage: (a) during fault without any protective measure; (b) during fault with PI controlled support from super-capacitor (–); FOSMC controlled support from super-capacitor (–).

Note that, when the fault occurs there is a huge short circuit current in the stator which induces high rotor currents which in turn increase the dc-link voltage very rapidly to a very high value (more than $2V_{dc}$). When using the PI controller (Fig. 4(b)), the dc-link voltage surge is mitigated and maintained near the reference value, however, the fluctuations are still significant thus leading to electromagnetic torque oscillations. Additionally, there is a significant dc-link voltage surge when the fault occurs which may also trigger the crowbar. When the FOSMC-based control strategy is activated, however, the fluctuations in the dc-link voltage are significantly reduced (Fig. 4(b). The dc link voltage is almost maintained at its nominal value and the voltage surge resulting from the fault is properly mitigated.

The GSC currents are depicted in Fig. 5. Note from Fig. 5(a) that the GSC current is still quite high despite the support from the super-capacitor when using the PI control. Whereas, the GSC current is significantly reduced with the proposed FOSMC control as shown in Fig. 5(b).

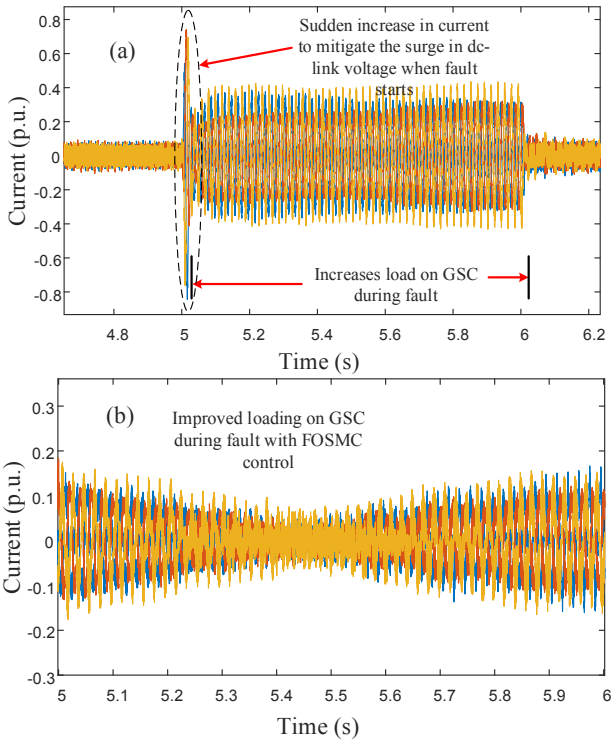

Fig. 5. GSC current during fault: (a) with PI controlled support from super-capacitor; (b) with FOSMC controlled support from super-capacitor.

Fig. 6 shows the current supplies from the super-capacitor. It shows that the super-capacitor absorbs significant current from the dc-link to support the voltage regulation. When the fault clears, there is still some voltage fluctuation which is also mitigated by the super-capacitor.

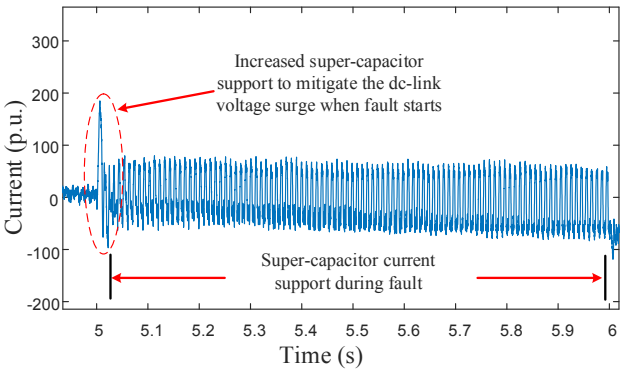

Fig. 6. Super-capacitor current with FOSMC during faulty condition.

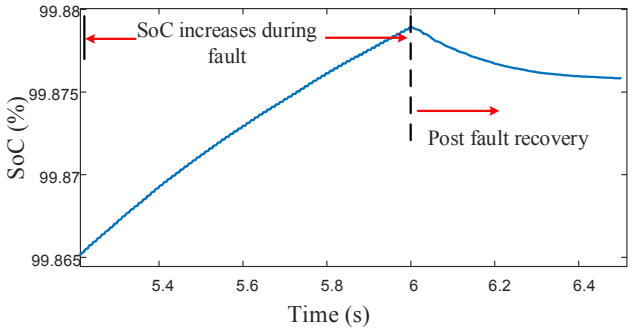

Fig. 7. Super-capacitor state of charge (SoC) with FOSMC control.

Fig. 7 shows the state-of-charge (SoC) of the super-capacitor. The SoC of the super-capacitor starts to rise upon fault occurrence and keeps rising during the fault since the super-capacitor absorbs the current to de-escalate the voltage surge. At 6 sec, the fault clears, therefore the SoC maintains a constant value. However, before that, there is a drop at SoC value since, there is a voltage drop in dc-link when the fault clears as shown in Fig. 4(a). At that moment, the super-capacitor works in the discharge mode to maintain the dc-link voltage.

The above results confirm that the proposed control strategy shows significant improvement in the stability of the back-to-back converter system. Additionally, the FOSMC controlled switching proves to be a lot more effective than the PI controlled switching in mitigating the transients with the supplemental energy storage.

6. CONCLUSION

This paper proposed a fractional order sliding mode-based approach for the converters of a DFIG-based wind energy system in a standalone power supply system. The proposed approach was shown to protect the converters from voltage surges during grid faults and regulate the dc-link voltage to near its rated value, thus bypassing the crowbar system and circumventing its drawbacks. Additionally, the proposed control strategy showed significant improvement in the stability of the back-to-back converter system. A comparison to a standard PI approach proved the FOSMC-approach to be a lot more effective in mitigating the transients with the supplemental energy storage. Additionally, it can also be considered to either smooth the power output in fluctuating wind conditions or regulate the frequency in response to sudden load variations.

Appendix

TABLE I
DFIG PARAMETER VALUES

Parameter	Value
Turbine inertia constant	4.32 s
Stator terminal voltage	400 V
DC link voltage	850 V
X_m	2.3Ω
R_s	0.023Ω
X_s	0.18 Ω
R_r	0.016 Ω
X_r	0.16 Ω

TABLE II
BIDIRECTIONAL CONVERTER PARAMETERS

Parameter	Value
Super-capacitor rated voltage	500 V
Super-capacitor capacitance	500 F
L	4.5 mH
C_1	1200 μF
C_2	1200 μF

REFERENCES

Abbey, C., Joos, G. (2006). Energy storage and management in wind turbine generator systems. *Proc. Int. Pow. El. Mot. Cont. Conf.*, pp. 2055-2056.

Pena, R., Clare, J.C., Asher, G.M. (1996) Doubly fed induction generator using back-to-back PWM converters and its application to variable-speed wind-energy generation, *IEE Proc. Elec. Pow. App.*, 143, pp. 231-241.

Aktarujjaman, M., Kashem, M. A., Ledwich, G. (2006). Smoothing output power of a doubly fed wind turbine with an energy storage system. *IEEE Int. Conf. on Power Elec., Drives Energy Sys.*, pp. 2-6.

Chen, Z. (2019). Wind Energy Conversion Systems. *Appl. Sci*., 9, pp. 3258.

Erlich, I., Wrede, H. Feltes, C. (2007). Dynamic behaviour of DFIG-based wind turbines during grid faults. *Power Conv. Conf.*, pp. 1195-1200.

Hu, J., Nian, H., Hu, B., He, Y., Zhu, ZQ. (2010). Direct active and reactive power regulation of DFIG using sliding-mode control approach. *IEEE Trans. Energy Convers.*, 25(4), pp. 1028–39

Jalilian, A., Naderi, S. B., Negnevitsky, Muttaqi, K. M. (2017). Controllable DC-link fault current limiter augmentation with DC chopper to improve FRT of DFIG. *IET Renew. Pow. Gen.*, 11(2), pp. 313-324.

Mellincovsky, M., Yuhimenko, V., Peretz, M., Kuperman, A. (2018). Analysis and control of direct voltage regulated active DC-link capacitance reduction circuit. *IEEE Trans. Power Elec.*, 33(7), pp.6318-6332.

Morshed, M.J., Fekih, A. (2019). A sliding mode approach to enhance the power quality of wind turbines under unbalanced grid conditions. *IEEE/CAA J. of Automatica Sinica*, vol. 6, no. 2, pp. pp. 566-574.

Morshed, M. J., Fekih, A. (2015). Integral terminal sliding mode control to provide fault ride-through capability to a grid connected wind turbine driven DFIG. *Proc. of IEEE Int. Conf. Ind. Tech.*, pp. 1059-1064.

Naderi, S. B, Negnevitsky, M., Jalilian, A., Hagh, M. T., and Muttaqi, K. M. (2017). Low voltage ride-through enhancement of DFIG-based wind turbine using DC link switchable resistive type fault current limiter. *Int. J. of Electrical Power & Energy Systems.* vol. 86, pp. 104-119.

NasimUllah, M., Asghar, A., Ibeas, A., Herrera, J. (2017). Adaptive fractional order terminal sliding mode control of a DFIG-based wind energy system. *IEEE Access*, 5, pp. 21368-21381.

Podlubny, I. (1999). *Fractional Differential Equations*. Academic Press, vol. 198, New York, NY, USA.

Raju, SK, Pillai, GN. (2016). Design and implementation of type-2 fuzzy logic controller for DFIG-based wind energy systems in distribution networks. *IEEE Trans. Sustain. Energy*, 7(1), pp. 345–53.

Tan, Y, Muttaqi, K. M., Meegahapola, L, and Ciufo, P. (2016). Deadband control of doubly-fed induction generator around synchronous speed. *IEEE Trans. Ener. Conv.*, vol. 31(4) pp. 1610-1621.

Xiong, L., Li, P., Ma, M., Wang, Z., Wang, J. (2020). Output power quality enhancement of PMSG with fractional order sliding mode control. *Int. J. of Electrical Power & Energy Systems*, vol. 115, pp. 105402.

Yang, B., Yu, T., Shu, H., Zhang, Y., Chen, J., Sang, Y., et al. (2018). Passivity-based sliding mode control design for optimal power extraction of a PMSG based variable speed wind turbine. *Renewable Energy*, vol. 119, pp. 577–89.

Yang, J., Fletcher, J., O'Reilly, J. (2010). A Series dynamic resistor-based converter protection scheme for DFIG during various fault conditions. *IEEE Trans. on Energy Convers.*, vol. 25., pp. 422 - 432.

Yang, N., Wu, C., Jia, R., Liu, C. (2016). Fractional-Order Terminal Sliding-Mode Control for Buck DC/DC Converter. *Mathematical Problems in Engineering*, vol. 2016, pp. 6935081.

Zhang, L., Jin, XM., Zhan, LY. (2011). A novel LVRT control strategy of DFIG based rotor active crowbar. *Proc. of Asia-Pacific power and energy engineering conference, Wuhan, China*, 25–28.

Zhang, Z., Li, Z., Kazmierkowski, MP., Rodriguez, J., Kennel, R. (2018). Robust predictive control of three-level NPC back-to-back power converters PMSG wind turbine systems with revised prediction. *IEEE Trans. Power Electronics*, 33(11), pp. 9588–98.